Article

Numerical Analysis of Unsymmetric Flatbak Trailing Edge Airfoil to Reduce Turbomachinery Noise in Power Generation Cycle

Hyungki Shin[1], Hogeon Kim[2], Taehyung Kim[3], Soo-Hyun Kim[1], Soogab Lee[4], Young-Jin Baik[1] and Gilbong Lee[1,*]

[1] Energy Efficiency and Materials Research Division, Korea Institute of Energy Research, Daejeon, 305-343, South Korea; hkeewind@kier.re.kr(H.S.); kishing@kier.re.kr(S.H.L); twinjin@kier.re.kr(Y.J.B.); giblee@kier.re.kr(G.L.)

[2] CD-adapco Korea, South Korea; hogeon.kim@cd-adapco.com

[3] Hyundai Heavy Industries Co.Ltd., South Korea; thk81@hhi.co.kr

[4] Seoul National University, Seoul, South Korea; solee@snu.ac.kr

* Correspondence: giblee@kier.re.kr; Tel.: +82-42-860-3293

Abstract: A turbomachinery is essential part in the power generation cycle. But, it is main noise source to annoy workers and users and to make environmental problem. Thus it is important to reduce this noise for operating the power generation cycle. This noise is created by flow instability on rotor blade trailing edge. An airfoil that becomes a section of a rotor blade of a rotating machine is manufactured as a blunt trailing edge (TE) with a round or flatback shape rather than the ideal sharp TE shape for the purposes of producibility and durability. This increases the tonal noise and flow-induced vibration at low frequency owing to vortex shedding behind TE when compared with a sharp TE. In order to overcome this problem, this study investigates the oblique TE shape using numerical simulation. In order to do so, the flow was simulated using large eddy simulation (LES) and the noise was analysed by acoustic analogy coupled with LES result. Once the simulation results were verified using the flatback airfoil measurements of Sandia National Laboratories, numerical prediction was performed for airfoils modified to have oblique trailing edge angles of 60°, 45°, and 30° to analyse the flow and noise characteristics. From the simulation results for an airfoil having an oblique TE, it could be seen that the vortex shedding frequency moves in accordance with the oblique angle and that the vortex shedding noise characteristics change according to this angle when compared to the flatback TE airfoil. Therefore, it is considered that modifying the flatback TE airfoil to have an appropriate oblique angle can reduce noise and change the tonal frequency to a bandwidth that is suitable for mechanical systems.

Keywords: power generation cycle; turbo machinery; turbine; compressor; blade; airfoil; noise

1. Introduction

A compressor and a turbine are essential components in the power generation cycle such as Rankine or Brayton cycle. A compressor or turbine makes high level noise that annoys users and causes environmental issues. Sometimes compressor operates under designed speed to reduce overall noise level[1]. It has a negative effect on efficiency and performance. For this reason, to reduce noise is one of essential problem for compressor and turbine operation in the power generation cycle. The main noise source of these machines is aerodynamic noise by rotor, screw, impeller or nozzle[2,3]. Thus, it is necessary to improve noise level with geometry design of airfoil and blade.

Airfoil shape -which is sectional geometry of blade- is an important design consideration not only for the fixed wings of aircraft but also for a variety of rotating machines such as compressors, turbines, pumps, propellers, and rotor blade [4,5]. Ideally, the trailing edge (TE) of an airfoil requires

Peer-reviewed version available at Energies 2017, 10, 872; doi:10.3390/en10070872

a sharp shape where the thickness is 0. However, practically, it is not easy to maintain a sharp trailing edge shape because of issues associated with damage during manufacturing and operation. Therefore, an airfoil is manufactured with a blunt TE in a round or flatback shape for blades of rotating machines (Figure 1) [6-10]. Also, a blunt TE in the blade root of a rotating machine has advantages in terms of structural strength owing to the increased cross-sectional area [11-13]. In addition, a flatback airfoil has the advantage of increased local lift coefficient [14].

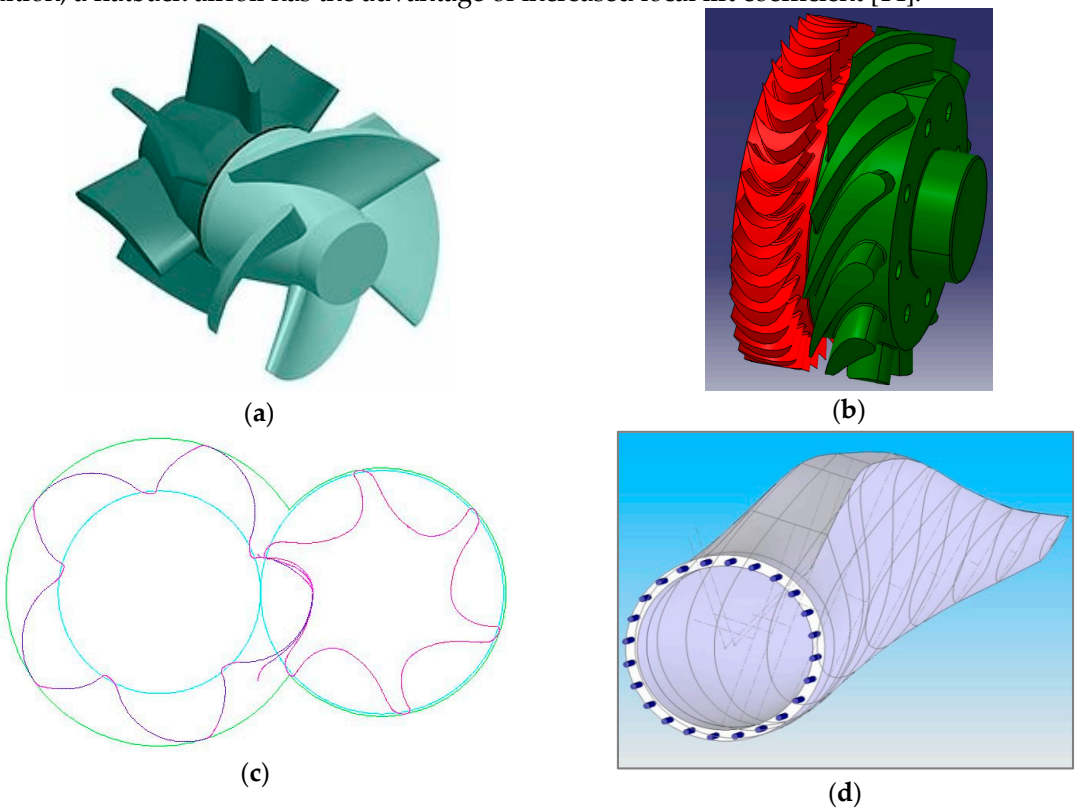

Figure 1. Rotating machine geometry (**a**) Axial fan; (**b**) Axial Impulse turbine; (**c**) Screw compressor (**d**) BSDS rotor blade[20]

However, an airfoil with a blunt or flatback TE shape increases pressure drag and tonal noise component at low frequency [15,16]. When airfoils with blunt or flatback TE shape are employed in turbines and compressor rotors, such tonal noise may act as one of the main noise sources [17,18]. This tonal noise is associated with the ringing of coherent structures near the trailing edge and involve the unsteady behaviours of counter-rotating streamwise vortices related to Karman vortex streets[19]. Such unsteady three-dimensional characteristics are related to the Reynolds number, turbulence intensity of the freestream flow, and turbulence components in the boundary layers near the TE[20]. In addition, the wake due to vortex shedding in the case of blunt TEs may not only result in resonance in turbines and compressor rotor blades but also cause structural problems in multi-stage compressors or turbines, as it can act as an unsteady loading in the next-stage blade [21-23]. Moreover, for cogwheel screw compressors, the tip cannot be manufactured with a sharp shape and potentially acts as a source of noise or vibration.

Many researches have been carried out to explain physical phenomena and to find prediction model of this tonal noise. Brooks and Hodgson[24] measured suggested some model for blunt and sharp TE airfoil noise. Blake and Gershfeld[25,26] showed that TE vortex shedding was pronounced on both symmetric and blunt TE geometries in their experiments. Prasad and Williamson[27] reviewed vortex dynamics related to the wakes of bluff body. Shannon and Morris[28] measured the wake behind blunt trailing edgy by PIV technique. Huerre and Monkewitz[29] also provided flow instability and wake flow of bluff body. However at present, despite of many researches, a complete description of this tonal noise phenomenon is still missing, partly owing to the limitations and shortcomings of classical hydrodynamic stability theory. For instance, spatial stability analyses

correctly predict the frequency of the most dominant tone[30], but they are unable to predict the tonal noise by a complex T.E. geometry of airfoil. Also, some researches were attempted to reduce this tonal noise. In an experimental studies of flatback airfoils, Berg and Zayas [31] designed a flatback root blade section with a thickness to chord length ratio of 0.1 and performed aerodynamic and acoustic tests in a wind tunnel. Kim et al. [32,33] performed numerical simulation of flatback airfoil aerodynamic noise using hybrid RANS-LES and acoustic analogy. They also predicted blunt TE vortex shedding noise by introducing a modified empirical formula. In another study, an attachment was fixed on the TE for noise reduction [34]. Barone et al. [35] reduced flatback airfoil noise by 4 dB using a splitter plate attached to the blunt TE. In their numerical studies of blunt TE airfoils, Stone et al. [36] achieved 5 dB noise reduction at an angle of attack of 5° by attaching a splitter plate behind the flatback wing; however, no experimental validation was reported. Although attachments such as splitters may reduce noise, they complicate the blade manufacturing process and reduce the service life. Therefore, there is a need for a TE shape treatment that considers producibility while reducing noise.

Toward this end, an oblique TE coupled with flatback geometry is considered to maintain the advantage of flatback TE shape and to reduce tonal noise. An appropriately shaped oblique TE may weaken the vortex shedding phenomenon at the lower surface and break vortex street behind TE, then eliminate tonal noise by reducing the interference via vortex offsetting, and change the frequency that generates flow-induced vibration. As mentioned before, although many endeavoured experiments and research about airfoil TE noise, it is still difficult to predict TE tonal noise of complex flatback TE geometry by previous model[37]. Thus, numerical approach was used to consider TE geometry effect of flatback airfoil to reduce this tonal noise and wake instability in this study.

TE flow and the noise generated by a TE cannot be analysed using the Reynolds-Averaged Navier Stokes (RANS) equation owing to accuracy problems [36]. For Computational Aero-Acoustics (CAA) using the Direct Numerical Simulation (DNS) method, accurate noise prediction can be expected albeit with a significant increase in the computing requirements because a very fine mesh and a highly accurate scheme is required with regard to time and space [38,39]. In the present work, a Large Eddy Simulation (LES) model and Ffowcs Williams-Hawkings(FW-H) acoustic analogy model were used to capture the wake instabilities and predict the noise radiated by a flatback TE. Large eddy simulation is a useful tool for general realistic turbulence problems. To reduce the calculation time, steady-RANS results were used for the initial condition of transient-LES calculation. The radiated sound was obtained by the FW-H model to predict dipole noise by pressure fluctuation on airfoil surface.

In this study, primarily, the accuracy of the numerical results was verified by using the analysis method described above with the noise measurement data [35] of the DU97W300 flatback airfoil tested by Sandia National Laboratories. Subsequently, to reduce the tonal noise of the flatback TE airfoil, the TE was modified with an oblique shape and the effects were analysed by verified numerical simulation.

2. Methodology

2.1. Large Eddy Simulation

The objective of this paper is to simulate blunt TE vortex shedding noise induced by exterior flow. The fluid has Newtonian flow characteristics such that the shear stress is proportional to the rate of change. This flow can be governed by the Navier-Stokes equation. The Navier-Stokes equation consists of five main equations, including one continuity equation, three momentum equations, and one energy conservation equation (Equations (1), (2), (3)).

$$\frac{\partial}{\partial t}\left(\int_V \rho dV\right) + \oint_A \rho \mathbf{v} \cdot d\mathbf{a} = \int_V S dV, \tag{1}$$

$$\frac{\partial}{\partial t}\left(\int_V \rho \mathbf{v} dV\right) + \oint_A \rho \mathbf{v} \otimes \mathbf{v} \cdot d\mathbf{a} = -\oint_A p\mathbf{I} \cdot d\mathbf{a} + \oint_A \mathbf{T} \cdot d\mathbf{a} + \int_V \mathbf{f}_b dV, \tag{2}$$

$$\frac{\partial}{\partial t}\left(\int_V \rho E dV\right) + \oint_A \rho H \mathbf{v} \cdot d\mathbf{a} = -\oint_A \dot{\mathbf{q}}'' \cdot d\mathbf{a} + \oint_A \mathbf{T} \cdot \mathbf{v} d\mathbf{a} + \int_V \mathbf{f}_b \cdot \mathbf{v} dV + \int_V S_E dV, \quad (3)$$

where p, ρ, $\mathbf{I}$, $\mathbf{T}$, and $\mathbf{f}_b$ denote the pressure, density, identity tensor, stress tensor and body force respectively. Every velocity component is included in vector $\mathbf{v}$.

The wake is major noise source of Blunt Trailing Edge airfoil. Thus, an accurate turbulence model is usually necessary in this case. For this reason, LES turbulence model was applied to this numerical simulation. LES involves large-scale analysis of turbulence, while the small-scale eddy is a modelling method. In contrast to the RANS equations, the equations that are solved for large eddy simulation are obtained by a spatial filtering rather than an averaging process. Each solution variable $\emptyset$(velocity compoents, pressure, etc.) is decomposed into a filtered value $\tilde{\emptyset}$ and a sub-filtered, or sub-grid, value $\emptyset'$ as

$$\emptyset = \tilde{\emptyset} + \emptyset', \quad (4)$$

The filtering of the generic instantaneous flow variable $\emptyset(t, x)$ is defined as

$$\tilde{\emptyset}(t, x) = \iiint_{-\infty}^{\infty} G(x - x', \Delta)\emptyset(t, x')dx', \quad (5)$$

Where $G(\mathbf{x}, \Delta)$ is a filter function characterised by a filter with $\Delta = (\Delta_x \Delta_y \Delta_z)^{1/3}$.

The filtered Navier-Stokes equation expressed in Cartesian coordinates can be expressed as Equation (6) and (7) .

$$\frac{\partial \rho}{\partial t} + \nabla \cdot (\rho \tilde{\mathbf{v}}) = 0, \quad (6)$$

$$\frac{\partial}{\partial t}(\rho \tilde{\mathbf{v}}) + \nabla \cdot (\rho \tilde{\mathbf{v}} \otimes \tilde{\mathbf{v}}) = -\nabla \cdot \tilde{p}\mathbf{I} + \nabla \cdot (\mathbf{T} + \mathbf{T}_t) + \mathbf{f}_b, \quad (7)$$

Where $\tilde{\mathbf{v}}$ and $\tilde{p}$ are the filtered velocity and pressure respectively.

Based on the eddy-viscosity model [40] of Boussinesq, the tensor is modelled as

$$\mathbf{T}_t = 2\mu_t \mathbf{S} - \tfrac{2}{3}(\mu_t \nabla \cdot \tilde{\mathbf{v}} + \rho k)\mathbf{I}, \quad (8)$$

Where $\mathbf{S}$ is the mean strain rate tensor and k is the subgrid scale turbulent kinetic energy.

As subgrid scale model, the Wall-Adapting Local-Eddy (WALE) [41] subrid scale model was applied.

2.2. Acoustic Analogy

Noise prediction is performed using the Ffowcs Williams-Hawkings(FW-H) equation [25]. This model calculate the far-field noise that is radiated from near-field data from a CFD result. The FW-H formulations are based on Farassat's Formulation 1A which is an extension of Lighthill's acoustic analogy [42]. Farassat's Formulation 1A is a non-convective form of FW-H for general subsonic source regions, including the impermeable formulation. In this study, impermeable surface that coincide with airfoil surface was applied for surface integral because the main noise of blunt T.E airfoil was generated by wake behind airfoil[43].

The FW-H equation is an exact rearrangement of the continuity and the momentum equations into the form of an inhomogeneous wave equation. The FW-H equation gives accurate results even if the surface of integration lies in the nonlinear flow region. It is based on the free-space Green's function to compute the sound pressure at the observer location, $\boldsymbol{x}$. The FW-H equation for pressure that is radiated into a medium at rest by a flow in a region or a set of surfaces is:

$$\mathrm{p}'(\mathbf{x}, t) = \mathrm{p}'_T(\mathbf{x}, t) + \mathrm{p}'_L(\mathbf{x}, t) + \mathrm{p}'_Q(\mathbf{x}, t), \quad (9)$$

The monopole, dipole, quadrupole terms are:

$$\mathrm{p}'_T(\mathbf{x}, t) = \frac{1}{4\pi}\left(\left(\frac{\partial}{\partial t}\right)\right) \int_S \left[\frac{Q}{(r(1 - M_r))}\right]_{ret} dS, \quad (10)$$

$$p'_L(\mathbf{x},t) = \frac{1}{4\pi}\left(\left(-\frac{\partial}{\partial x_i}\right)\right)\int_S \left[\frac{L_i}{(r(1-M_r))}\right]_{ret} dS, \tag{11}$$

$$p'_Q(\mathbf{x},t) = \frac{1}{4\pi}\left(\left(\frac{\partial^2}{(\partial x_i)(\partial x_j)}\right)\right)\int_V \left[\frac{T_{ij}}{(r(1-M_r))}\right]_{ret} dS, \tag{12}$$

With

$$Q = \rho_0\left(\left(1-\frac{\rho}{\rho_0}\right)v_i + \frac{\rho u_i}{\rho_0}\right), \tag{13}$$

$$L_i = \left((p-p_0)\delta_{ij} - \sigma_{ij}\right)n_i + \rho u_i(u_n - v_n), \tag{14}$$

$$T_{ij} = \rho u_i u_j + \delta_{ij}[(p-p_0) - c_0^2(\rho-\rho_0)] - \sigma_{ij}, \tag{15}$$

Where

u_i is the fluid velocity components in the x_i direction.
u_n is the fluid velocity component normal to the surface.
v_i is the fluid velocity components in the x_i direction.
v_n is the surface velocity component normal to the surface.
v_n is the surface normal vector.
n_i is the viscous stress tensor.
ρ_0 is the far field density.

The space derivatives from Equation (10) and (11) are transformed into time derivatives and afterwards, the time derivatives at the observer locations are moved into the integrals.

When the integration surface coincides with the body, the total surface term, $p'_S(\mathbf{x},t)$, resulting from the sum of the Thickness Surface Term and the Loading Surface Term like :

$$p'_S(\mathbf{x},t) = p'_T(\mathbf{x},t) + p'_L(\mathbf{x},t), \tag{16}$$

Farrassat's Formuation 1A is for general subsonic source regions, for general far-field noise prediction[44,45]. This formulation is following Equation (17) and (18).

$$p'_T(\mathbf{x},t) = \frac{1}{4\pi}\left(\int_{(f=0)}\left[\frac{\rho_0(\dot{U}_n+U_{\dot{n}})}{r(1-M_r)^2}\right]_{ret} dS + \int_{(f=0)}\left[\frac{\rho_0 U_n[r\dot{M}_r + a_0(M_r-M^2)]}{r^2(1-M_r)^3}\right]_{ret} dS\right), \tag{17}$$

$$\begin{aligned} p'_L(\mathbf{x},t) = \frac{1}{4\pi}\Bigg(&\frac{1}{a_0}\int_{(f=0)}\left[\frac{\dot{L}_r}{r(1-M_r)^2}\right]_{ret} dS + \int_{(f=0)}\left[\frac{(L_r-L_M)}{r^2(1-M_r)^2}\right]_{ret} dS \\ &+ \frac{1}{a_0}\int_{(f=0)}\left[\frac{L_r\left[r\dot{M}_r + a_0(M_r-M^2)\right]}{r^2(1-M_r)^3}\right]_{ret} dS\Bigg) \end{aligned} \tag{18}$$

Where :

$$L_i = \left((p-p_0)\delta_{ij} - \sigma_{ij}\right)n_i + \rho u_i(u_n - v_n), \tag{19}$$

$$M_i = U_i/a_0, \tag{20}$$

$$r = x_{observer} - y_{face}, \tag{21}$$

$f = 0$ represents the emission surface and is made coincident with a body(airfoil surface), impermeable surface. If the data surface coincides with a solid surface, then the normal velocity of the fluid is the same as the normal velocity of the surface : $u_n = v_n$. In this case, Equation (17) and (18) correspond to the Impermeable FW-H Surface type.

The major task in evaluating the FW-H integrals is how to account for the time-lag between emission and reception times. The advanced time algorithm looks forward in time to see when the observer perceives the currently generated sound waves[46]:

- The procedure starts with a sequence of emission times (conveniently taken as the flow times).
- The source strengths are calculated (thickness surface noise and loading surface noise) at all source elements (faces of the integration surfaces) for a given emission time.
- The contribution of the sources is interpolated in the far-field time domain to build the sound signal.

The total sound pressure that the observer perceives consists of the contribution from all source elements. The sound pressure at the receiver is obtained by accumulating the arriving signals in time slots. The overall observer acoustic signal is found from the summation of the acoustic signal from each source element of the FW-H surface during the same source time

2.3. Numerical Conditions

A commercial CFD S/W, Star-CCM+, was used for the numerical simulation for noise analysis. For an accurate pressure fluctuation value in the time domain for noise analysis, LES was applied to the turbulence model while the results from the RANS model were used as the initial condition for the LES model in order to shorten the calculation time.

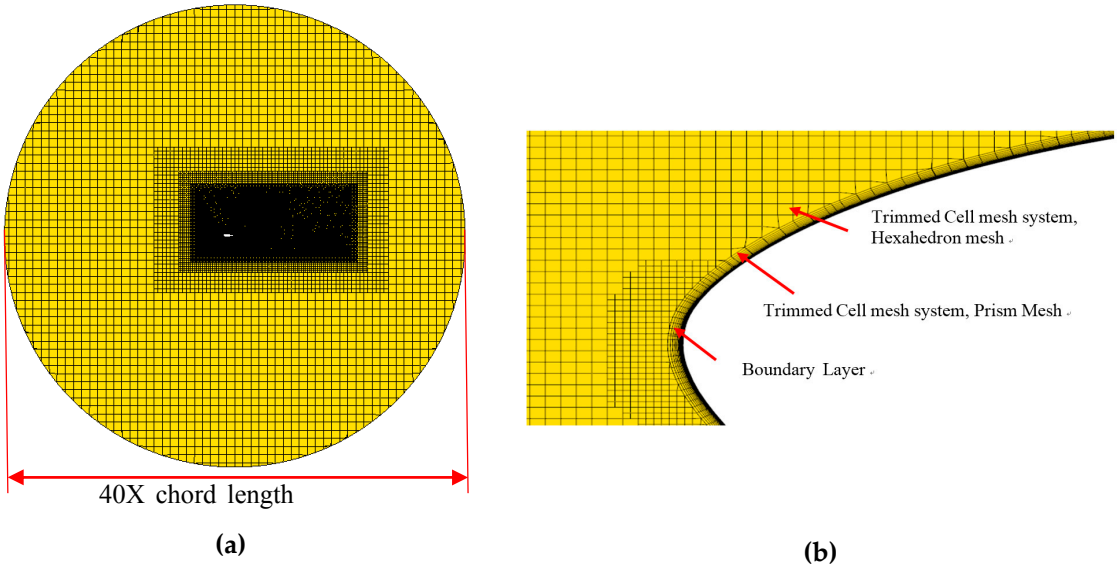

Figure 2. Grid system for RANS and LES analysis (**a**) Whole gird structure; (**b**) Grid structure near airfoil wall

For the grid resolution and structure for CFD calculation, a grid system for LES model analysis was created, and the same grid system was applied to the RANS model. The entire calculation area was created as a circle as shown in Figure. 2(a), with a diameter that is 40 times the chord length. The chord length of the CFD model was identical to that of the wind tunnel test model (0.91 m) while the spanwise length was set to two times the chord length(1.82m) in order to satisfy the LES grid criteria [47] suggested by Baggett. The basic grid structure is a trimmed cell mesh and was created as the block-structured grid type. The fluid region was created as a hexahedron mesh and the area coming in contact with the boundary layer mesh was made with prism mesh (Figure 2(b).) The area around leading edge (LE), which is the stagnation point, has alignment of cells created to be 0.275% of the chord length, forming a grid in which the cell size increases with the distance from the airfoil two-fold in a stepwise manner from 0.55% of the chord length to 70.4%. The boundary layer area was created by overlapping 20 layers in the normal direction on top of the airfoil surface. For precise simulation of the boundary layer flow, the cell thickness in the first layer of the boundary layer area was set to $2.94*10^{-4}$ times the airfoil chord length with a stretching factor of 1.2, so that the boundary layer was created until the 20 layers had a thickness of 5.5% of the chord length (Figure 3). Total mesh

Preprints (www.preprints.org) | NOT PEER-REVIEWED | Posted: 19 May 2017 doi:10.20944/preprints201705.0146.v1

Peer-reviewed version available at Energies 2017, 10, 872; doi:10.3390/en10070872

number was 17millions for each airfoil. Figure 4. Shows the resulting y+ distribution on the surface of the airfoil after calculation was converged. Around the TE area where the vortex shedding occurs, the values are maintained under 2. This shows that mesh size on the wall is sufficient for this problem.

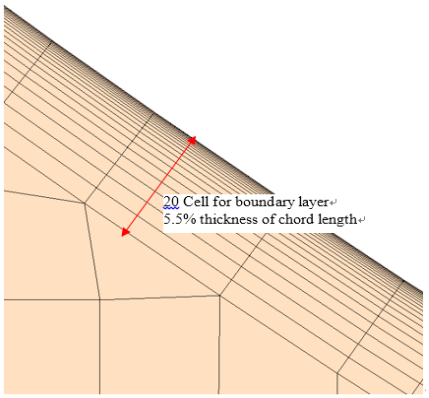

Figure 3. Boundary layer cell structure

In the turbulence model, the SST (Menter) K-omega model was applied for the RANS model to calculate the initial value for LES analysis [48]. In the LES model, the WALE model [41] was applied for the SGS model. Both the RANS model and the LES model used the all y+ treatment method as the wall function while the third-order Monotonic Upstream-Centered Scheme for Conservation Laws (MUSCL) scheme was applied as the convection scheme in spatial discretization. In LES interpretation, the time discretization used $5.0*10^{-5}$ s interval in the second order while simulation was conducted for 0.8 s for adequate convection of vortex shedding flow in the TE for the condition with a chord length of 0.92 m and inflow speed of 28.7 m/s. The noise in the far field caused by turbulence and arbitrary motion was calculated using the FW-H equation [25] based on Lighthill's acoustic analogy [42].

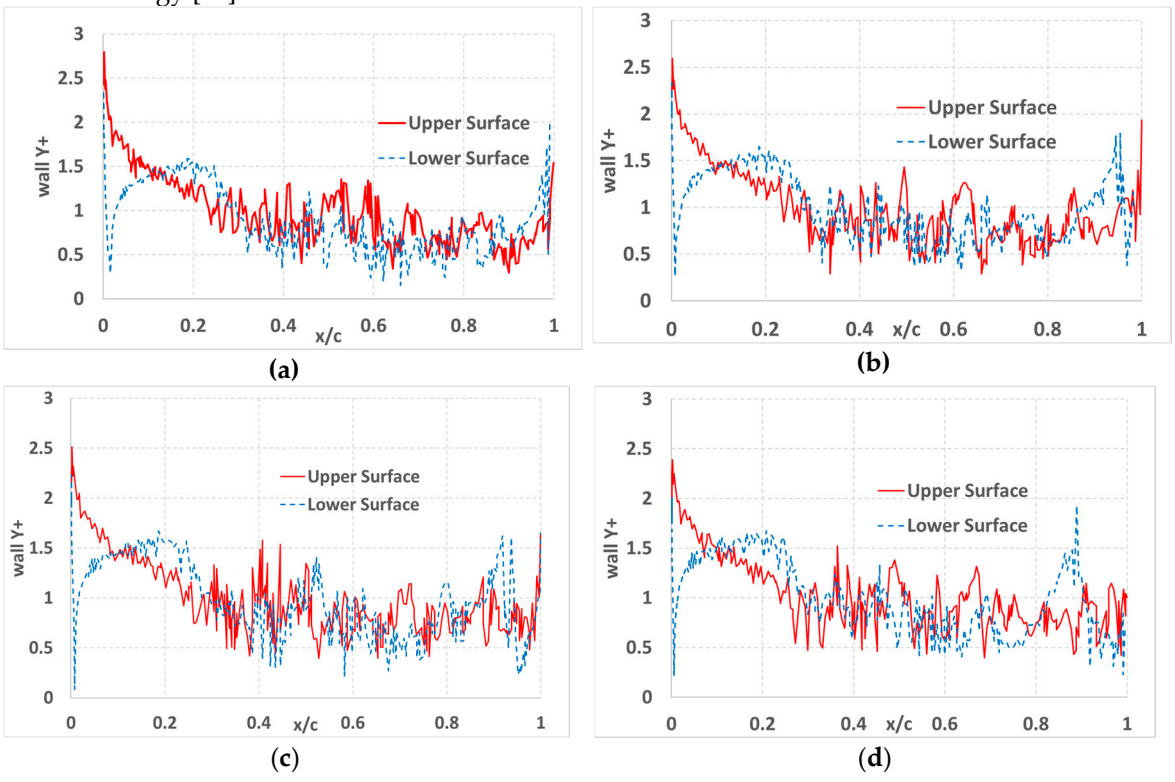

Figure 4. Wall y+ distribution(Geometric AOA=5.1°, Re.No.=2.4&10^6) (**a**) Flatback; (**b**) Oblique60; (**c**) Oblique45; (**d**) Oblique30

2.4. Test Cases

The numerical analysis results were verified on the basis of a DU97-Flatback airfoil to examine the noise effects on airfoils having flatback and oblique TEs. After confirming the reliability of the applied method and calculation results by comparing the calculation results and wind tunnel test results for the DU97-Flatback airfoil, the noise effects of the TE were analysed by modifying the TE shape to oblique.

The DU97-Flatback airfoil is the flatback TE version of the DU97-W-300 airfoil, with the flatback shape of the TE being 10% of the chord length (Figure 5). The calculation results for this airfoil were compared with the measurement data obtained at the Virginia Tech Stability Wind Tunnel by Sandia National Laboratories [35]. The wind tunnel test model for the airfoil has a chord length of 0.914 m and a span length of 1.8 m. For validation of the aerodynamic results, the numerical results were compared with the Cp distribution on the surface of the airfoil measured under an effective angle of attack (AOA) of 4.4°, flow speed of 28.7 m/s, and case of geometric AOA of 5.1°, flow speed of 58.6 m/s. For validation of the aero-acoustic result, the calculation results were compared with the results of the 1/12th octave band for the noise measured at a geometric AOA of 5.1° and flow speed of 44 m/s(Re. No. =2.4*10^6). The measurement point was 3.04 m from the top of the airfoil.

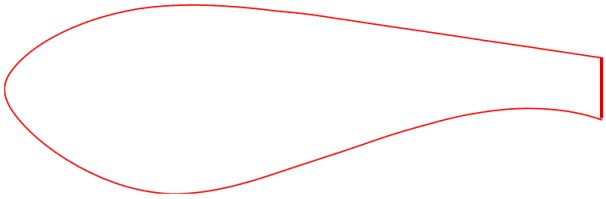

Figure 5. Geometry of DU97W300 Flatback airfoil

In order to examine the noise effects of the TE shape, numerical prediction was performed for a TE having a lower surface with an oblique shape, as shown in Figure 6. While maintaining 2% of the chord length for the flat portion of the TE so that the load path can be formed [49], the TE shape was created with slopes of 60°, 45°, and 30°. The definition of the oblique angle is shown in Figure 6 (b), and the comparison of the TE shape with the DU97W300 flatback airfoil is shown in Figure 6(a). For this airfoil shape, the noise spectrum was compared by creating a grid and performing numerical analysis as described in Section 2.3. As for the numerical analysis condition, a geometric AOA is 5.1° and flow speed is 44 m/s(Re. No. =2.4*10^6) as the same condition for noise measurement.

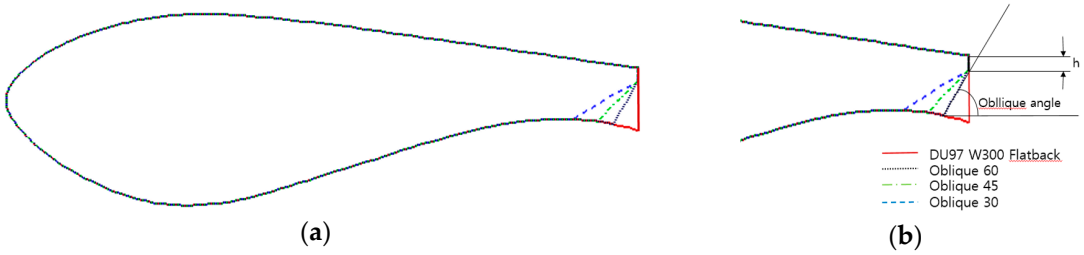

Figure 6. Oblique TE airfoils (a) Airfoil geometry comparison; (b) Oblique angle definition and TE comparison

3. Results and Discussion

3.1. Validation of Aerodynamic and Aero-acoustic Restults

In order to verify the accuracy of the numerical results, a comparison was made with the untrip condition data [35] for the DU97-Flatback airfoil from the Sandia National Laboratories wind tunnel measurements.

For quantitative analysis of the aerodynamic simulation, the pressure coefficient was compared by conducting numerical analysis for an effective AOA of 4.4° with flow speed of 28.7 m/s and Re. No. = 1.6*10^6, and for a geometric AOA of 5.1° with a flow speed of 58.6 m/s and Re. No. = 3.2*10^6. Here, the pressure coefficient (Cp) is defined as in Equation (22).

Preprints (www.preprints.org) | NOT PEER-REVIEWED | Posted: 19 May 2017 doi:10.20944/preprints201705.0146.v1

Peer-reviewed version available at Energies 2017, 10, 872; doi:10.3390/en10070872

$$C_p = \frac{P - P_\infty}{\frac{1}{2}\rho U_\infty^2} \tag{22}$$

Figure 7 shows the Cp distribution and comparison on the airfoil surface measured under $\alpha_{eff} = 4.4°$, Re. No. = 1.6*10⁶. The x-axis shows the normalized chord length while the y-axis shows the -Cp values. In this case, the Sandia National Laboratories test results were corrected with an effective AOA of 4.4° while the CFD simulation was calculated by setting the geometric AOA= 4.4°. LES analysis results overall match the test values well but show a slight difference with the LE and TE regions of the upper surface. In the wind tunnel test, transition was occured from the laminar boundary layer to the turbulent boundary layer on the LE region, and such an error is a result of the fact that LES analysis basically assumes fully turbulent flow for the entire numerical domain. Therefore, slight over-prediction is observed for -Cp of the upper surface near the LE area compared to the experimental value, but the location of the apex is predicted relatively accurately with values in the range of 20%~25%.

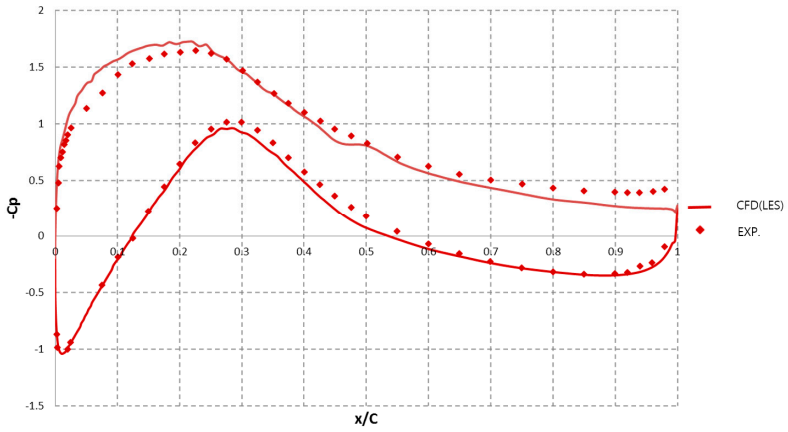

Figure 7. Comparison of the pressure coefficient Cp between the CFD prediction and experimental data (Effective AOA = 4.4°, Re. No. =1.6*10⁶)

Figure 8 shows the Cp distribution comparison of geometric AOA of 5.1°, Re. No. = 3.2*10⁶. In the case of the Sandia National Laboratories test, the test conditions are not corrected by effective AOA and only [35] geometric AOA is indicated; the same goes for noise measurement, which is described later, as it is also indicated in geometric AOA. Therefore, the AOA experienced by the airfoil in an actual test is smaller than 5.1°; as such, when the geometric AOA was calculated with 5.1° in CFD analysis, the -Cp value in the upper surface turned out to be greater than the measured value , and the error also increased.

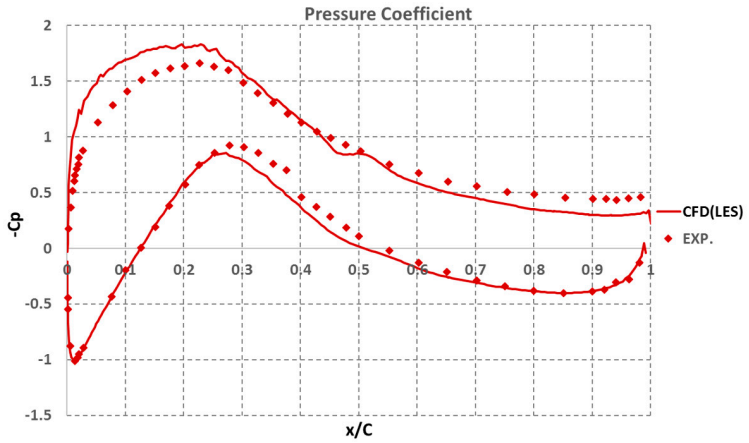

Figure 8. Comparison of the pressure coefficient Cp between the CFD prediction and experimental data (Geometric AOA = 5.1°, Re. No. =3.2*10⁶)

Preprints (www.preprints.org) | NOT PEER-REVIEWED | Posted: 19 May 2017 doi:10.20944/preprints201705.0146.v1

Peer-reviewed version available at Energies 2017, 10, 872; doi:10.3390/en10070872

The qualitative overview on flow can be seen in Figure 9 and Figure 10. Figure 9 shows the iso-surface of the Q=100/s^2 value for Q-criterion while Figure 10 shows the non-dimensional vorticity contour. All calculation conditions are geometric AOA of 5.1°, Re. No. = 2.4*10^6 of the same as noise measurement condition. The vorticity occurring in the boundary layer of the TE flows out to the back, creating a turbulent vortex street and a visible wake pattern. The eddy created in the upper and lower surfaces is convected downstream, creating a 2D coherent structure, which also becomes the primary mechanism of generation for the vortex shedding noise in the case of a blunt TE [50]. Figure 9 and 10 clearly show a trend similar to that of the results from the experiment by Shannon and Morris[28].

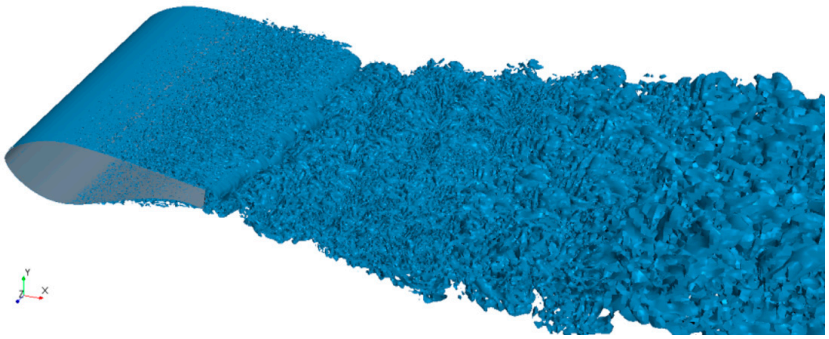

Figure 9. Visualization of the Q-criterion. Iso-surface Q=100/s^2(Geometric AOA = 5.1°, Re. No. =2.4*10^6)

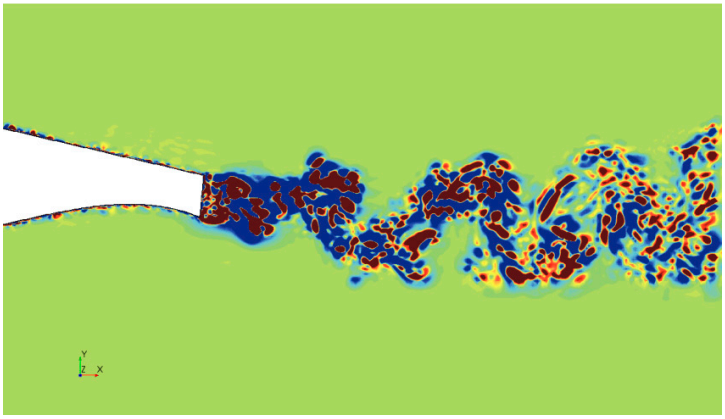

Figure 10. Instantaneous Q-criterion contour(Geometric AOA = 5.1°, Re. No. =2.4*10^6)

For the verification on noise analysis, a comparison was made with the data at a flow speed of 44 m/s, which clearly shows the components of tonal noise caused by the vortex shedding of the blunt TE. For the angle of attack, for the reason previously mentioned, it is given in the Sandia report as the geometric angle of attack [35], and as the effective angle of attack is not accurately known, an AOA of 5.1° was used in the LES analysis as well as for comparison. Figure 11 shows the distribution of the Instantaneous Acoustic Pressure calculated using Equation (23). In this figure, the value of the acoustic pressure is large in the trailing edge and vortex shedding area, which clearly shows that the main noise sources are TE and wake.

$$\text{Acoustic Pressure} = P_{s,t} - P_{average,calculation\ time} \quad (23)$$

Figure 12 shows the 1/12th octave band noise comparison between the measurement and the numerical analysis result. It can be seen that the numerical simulation result and measurement match well. Overall, the numerical result are predicted to be 1~4 dB higher than the measurement; this is believed to be because the effective AOA of the airfoil in the actual wind tunnel test is smaller than 5.1°, which is the value used in the numerical analysis, resulting in slightly higher numerical result compared to actual measurement. However, both the numerical result and the measurement

Preprints (www.preprints.org) | NOT PEER-REVIEWED | Posted: 19 May 2017 doi:10.20944/preprints201705.0146.v1

Peer-reviewed version available at Energies 2017, 10, 872; doi:10.3390/en10070872

effectively show the tonal noise components caused by vortex shedding in the blunt TE at a bandwidth of 121 Hz, and the Sound Pressure Level (SPL) values also match well. The peak Strouhal number calculated with TE thickness, flow speed, and peak frequency is 0.251; this value also agrees well with the value suggested by Blake [50] and Brooks, Pope, and Marcolini [51].

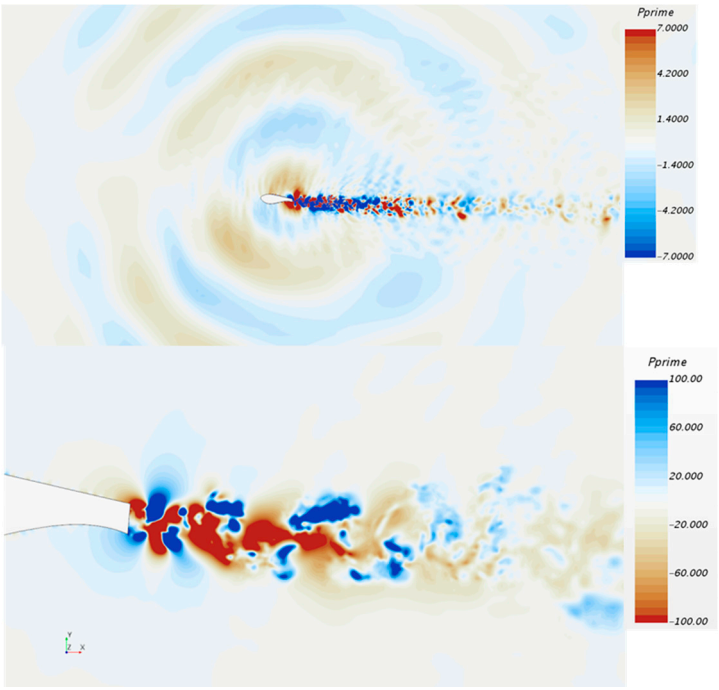

Figure 11. Acoustic pressure contour(Geometric AOA = 5.1°, Re. No. =2.4*10^6)

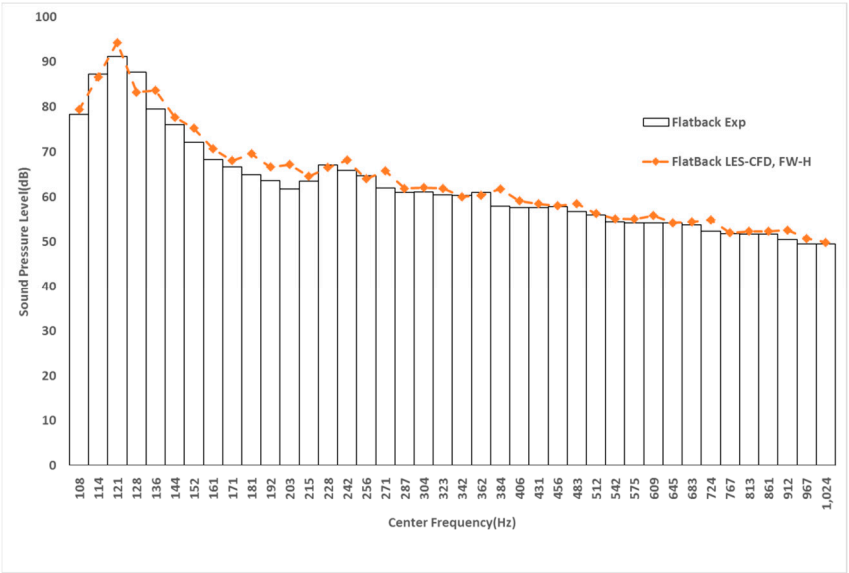

Figure 12. Noise comparison between measurement and calculation(Geometric AOA = 5.1°, Re. No. =2.4*10^6)

As shown above, the numerical simulation result match well with the measurement. This shows that the suggested numerical method yields reliable and significant results for aerodynamics and noise analysis using the blunt TE airfoil under the given conditions. Although there is an error between the geometric AOA and effective AOA, the difference is negligible. As meaningful results can be obtained by comparing the noise caused by the TE geometry at the same AOA, numerical analysis according to TE Geometry was performed for an AOA of 5.1° and Re. No. = 2.4*10^6.

3.2. Noise Analysis of Oblique Trailing Edge Airfoils

As mentioned in Section 2.4, in order to reduce TE tonal noise by breaking vortex street behind TE, calculations were made by changing the oblique angle to 60°, 45°, and 30° while maintaining the flatback geometry to 2% of the chord length in the TE (Figure 6). Figure 13 shows the noise comparison at 1/12th octave band about four TE shape. When examining the frequency component, it can be seen that the tonal noise component frequency moves to the high frequency zone as Flatback approaches Oblique30. Moreover, for Oblique30, only main tonal noise component exists and the second harmonic component is not really visible but the second harmonic for the fundamental frequency is clearly visible for Oblique60 and Oblique45. This is because the cause of the harmonic component is the wake vortex street periodicity, but for Oblique30, the second harmonic component is weakened as the wake street of the vortex shedding breaks down earlier than that in the case of Oblique60 and Oblique45.

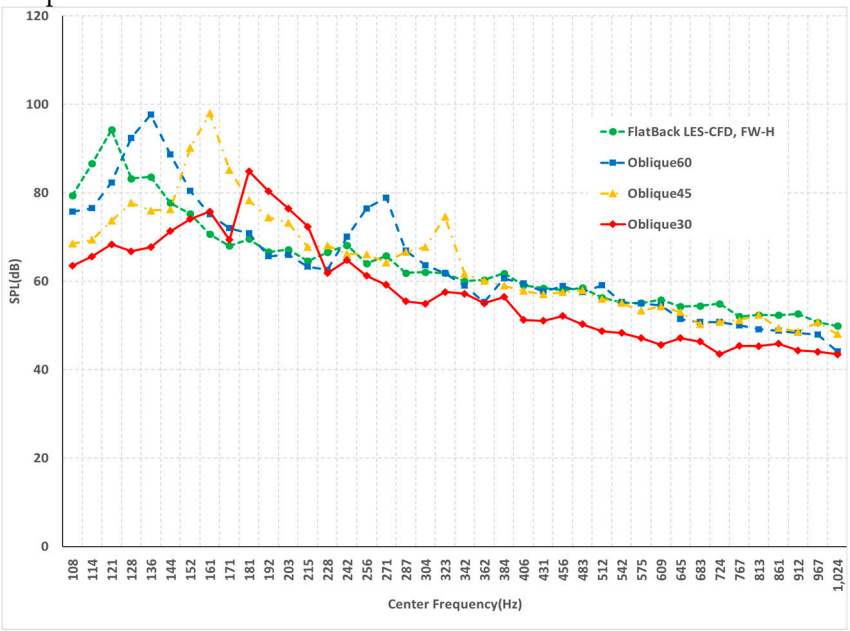

Figure 13. 1/12th octave band noise calculation of oblique TE airfoils(Geometric AOA = 5.1°, Re. No. =2.4*10^{6})

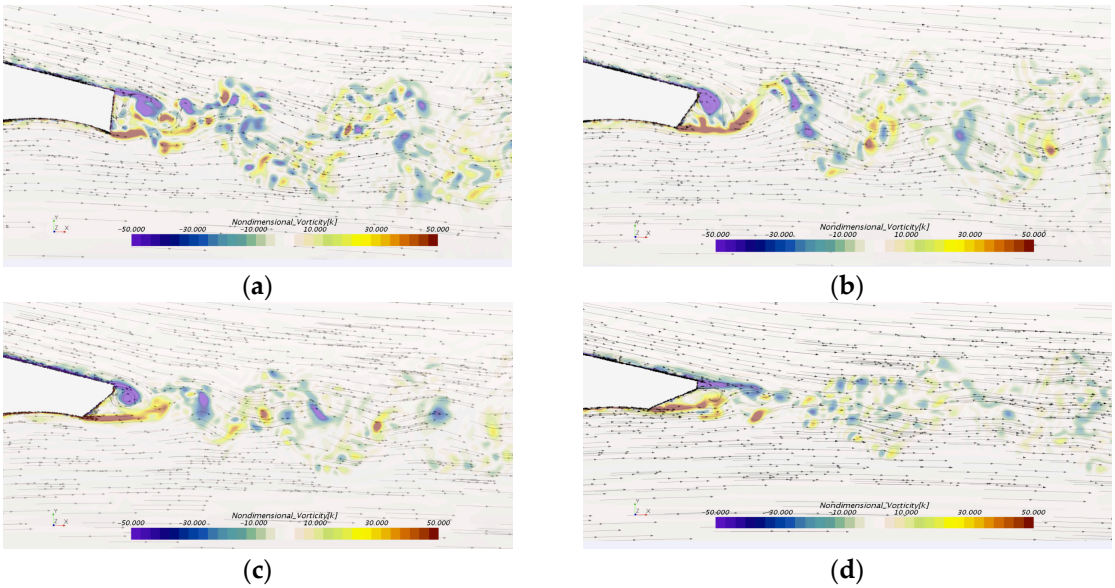

Figure 14. Non-dimensional vorticity contour & streamline (Geometric AOA=5.1°, Re.No.=2.4&10^{6}) (**a**) Flatback; (**b**) Oblique60; (**c**) Oblique45; (**d**) Oblique30

For SPL, the tonal noise level was nearly the same for Oblique60 and Oblique45, compared with the Flatback TE airfoil. In comparison, for Oblique30, the tonal noise component was reduced significantly compared to the Flatback TE airfoil. The cause can be determined upon examining the vortex shedding behind airfoil trailing edge. Figure 14 shows the non-dimensional vorticity contour and streamline around the airfoil TE. For an airfoil with a flatback trailing edge shape, vortex shedding occurs strongly in the upper and lower surfaces. For Oblique60 and Oblique45 with oblique angles of 60° and 45°, respectively, the vortex shedding observed was similar to the case of the flatback airfoil in the upper and the lower surface of the TE. Streamline shows circulation clearly upper side of TE in these cases. Moreover, as the vortices convected backward are clearly separated from each other, the tonal noise component increases compared to that of the flatback airfoil with a clear harmonic component. For Oblique30, the coherent structure is destroyed as the vortex occurring in the upper surface and the weakening vortex shedding in the lower surface offset each other. Also, it reduces wake instability and make streamline smooth. It can be seen vertical velocity fluctuation behind TE. Figure 15(a) shows vertical velocity power spectral density along the chord behind TE. X axis shows spatial frequency and Y axis is power spectral density in log scale. The peak and overall level is reduced for Oblique30 when compared with other cases.

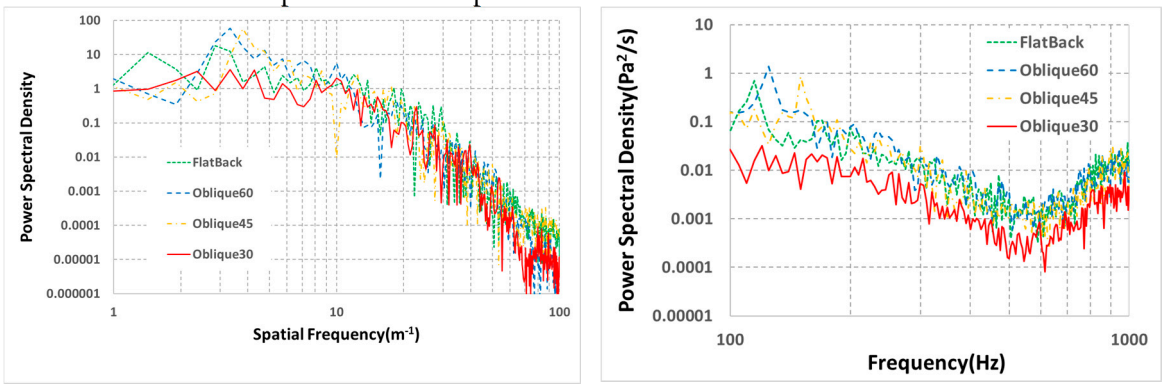

(**a**) (**b**)

Figure 15. Power spectral density behind TE (Geometric AOA=5.1°, Re.No.=2.4&10^6) (**a**) Vertical velocity PSD along the chord behind TE; (**b**) Pressure PSD behind TE point

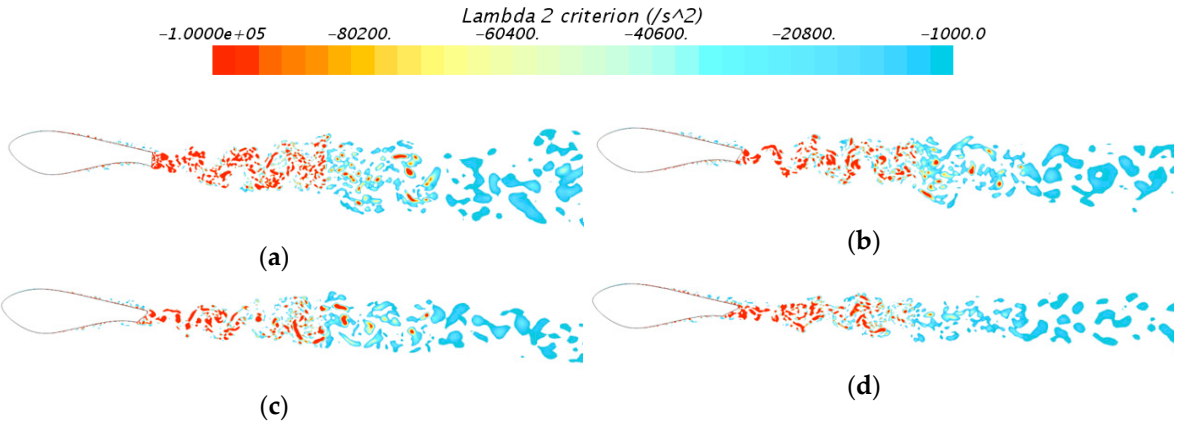

(**a**) (**b**)

(**c**) (**d**)

Figure 16. Lambda2 criterion (Geometric AOA=5.1°, Re.No.=2.4&10^6) (**a**) Flatback; (**b**) Oblique60; (**c**) Oblique45; (**d**) Oblique30

Therefore, for Oblique30, tonal noise could be significantly reduced compared to the flatback airfoil. This becomes clearer when the frequency component of the pressure fluctuation is observed downstream. Figure 15(b) shows the power spectral density of the pressure fluctuation at the location that is 3.4 times the chord length from the aerodynamic centre towards the wake direction. All of Flatback, Oblique60, and Oblique45 show a strong peak for the tonal noise frequency component while Oblique30 does not generate a peak. The strength of the peak also shows stronger characteristics for Oblique60 and Oblique45 than for Flatback. When observing the vorticity of the

wake expressed as the Lambda2 Criterion (Figure 16), Flatback shows a widely spread wake area while Oblique30 shows the smallest area. For Oblique60 and Oblique45, the area is small but they both show a clear and strong distribution of vorticity in the TE area. This explains the characteristics of tonal noise seen in the noise distribution of the 1/12th octave band.

4. Conclusion

This study investigated the noise effects on an airfoil TE having a flatback shape and an oblique angle combined to flatback geometry. Because it is difficult to calculate the noise level for complex TE shape analytically, the LES method and acoustic analogy were combined to numerically predict the vortex shedding flow and tonal noise for these airfoils. This method was verified with empirical data and accurately predicted the noise generation mechanism, peak frequency, and the SPL at peak frequency.

Based on these results and with the same numerical method, the vortex shedding flow and the vortex shedding noise were numerically predicted for an airfoil with a TE having oblique angles of 60°, 45°, and 30° that have flatback area. The results of prediction showed that the centre frequency of the tonal noise increased towards higher frequencies as the oblique angle decreased to 30° in the flatback case. For the SPL at peak frequency, the values are either nearly the same or slightly greater than that for the flatback TE in the case of oblique angles of 60° and 45° while a clear second harmonic component is also visible. An oblique angle 30° showed clear tonal noise reduction compared with the flatback TE

Therefore, for a flatback TE, the centre frequency of the tonal noise can be moved by changing the TE shape by combining oblique angle. This can also be used as a means to avoid the flow-induced resonance due to vortex shedding in rotors and blades. For the consideration of noise reduction, as with the prediction results above, different patterns were observed depending on the oblique angle. The results of this study show that an inadequate angle cannot contribute to noise reduction when changing the flatback shape to oblique shape for the purpose of noise reduction, and that the oblique angle must be less than 30° to break the wake street of the vortex shedding. In conclusion, when an adequate oblique angle is applied to a flatback TE, noise reduction can be achieved and the tonal frequency can be changed to a bandwidth that is suitable for mechanical systems.

Acknowledgments: This work was jointly supported by the Energy Efficiency & Resources Core Technology Program of the Korea Institute of Energy Technology Evaluation and Planning (KETEP), granted financial resource from the Ministry of Trade, Industry & Energy, Republic of Korea (No. 20132010101780) and Development Program of the Korea Institute of Energy Research (KIER B7-2414).

Author Contributions: Dr. H. Shin, Dr. T. Kim, Dr. S. Lee and Dr. SH Kim conceived the research idea and oblique TE airfoil for reducing vortex shedding. Dr. Shin, Dr. SH Kim and Dr. T.Kim designed detail TE geometry. Dr. Shin and Dr. H. Kim performed numerical simulation. Dr. Shin, Dr. H.Kim, Dr. S. Lee, Dr. YJ. Baik and Dr. G. Lee analyzed data and numerical results. All authors have contributed to the writing, editing and revising of this manuscript.

Conflicts of Interest: The authors declare no conflict of interest. The founding sponsors had no role in the design of the study; in the collection, analyses, or interpretation of data; in the writing of the manuscript, and in the decision to publish the results.

References

1. Lowson, M.V. Reduction of Compressor Noise Radiation, *The Journal of the Acoustical Society of America* **1968**, *43*, 37-47.
2. Tyler, J.; Sofrin, T. Axial Flow Compressor Noise Studies. *SAE Technical Pape*r 620532, **1962,** doi:10.4271/620532.
3. Horlock, J.H. Turbomachinery Noise Technology. *J. Fluids Eng* **1975**, *97(3)*, 283-284.
4. Thompson, B.E. ; Whitelaw, J.H. Flow-around airfoils with blunt, round, and sharp trailing edges. *Journal of Aircraft*,**1988**, *25(4)*, 334-342.

Peer-reviewed version available at Energies 2017, 10, 872; doi:10.3390/en10070872

5. Sant, R.; Ayuso, L. ; Meseguer, J. Influence of open trailing edge on laminar aerofoils at low Reynolds number. 49th AIAA Aerospace Sciences Meeting including the New Horizons Forum and Aerospace Exposition, Orlando, Florida, 2011.
6. https://en.wikipedia.org/wiki/File:Axial_geometry.jpg (accessed 04 April 2017).
7. Herrig, L.J. ; Emery, J. C. ; Erwin, J. R. Effect of section thickness and trailing edge radius on the performance of NACA 65-series compressor blade in cascade at low speeds. NACA RM L6651j16, 1951.
8. Emery, J.C. ; Herrig, L.J. ; Erwin J.R. ; Felix, A.R. Systematic two-dimensional cascade tests of NACA 65-series compressor blades at low speeds. NACA-RM-L54H18a, 1958.
9. Suder, K.L. ; Chima, R.V. ; Strazisar A. J. ; Roberts, W. B. The effect of adding roughness and Thickness to a transonic axial compressor rotor. *Journal of Turbomachinery*, **1995**, *117(4)*, 419-505.
10. Roelke, R.J. ; Haas, J.E. The Effect of Rotor Blade Thickness and Surface Finish on the Performance of a Small Axial Flow Turbine. *J. Eng. Power* ,**1983**, *105(2)*, 377-382.
11. Ghedin, F. Structural Design of a 5 MW Wind Turbine Blade Equipped with Boundary Layer Suction Technology - Analysis and lay-up optimisation applying a promising technology. MASTER OF SCIENCE THESIS, TUDelft, Delft, 2010.
12. van Dam, C.P. Research on thick blunt trailing edge wind turbine airfoils. 2008 wind turbine blade workshop Sandia National Laboratories, Albuquerque, New Mexico, 2008.
13. Jackson, K.J. ; Zuteck, M.D. ; van Dam C.P. ; Berry, D. TPI Composites, Innovative Design Approaches for Large Wind Turbine Blades – Final Report. *Wind Energy*, **2005**, *8(2)*, 141-171.
14. van Dam, C.P. ; Mayda, E.A.; Chao, D.D. Computational Design and Analysis of Flatback Airfoil Wind Tunnel Experiment. SANDIA REPORT, SAND2008-1782, 2008.
15. Cooperman, A.M. ; McLennan, A.W. ; Chow, R. ; Baker, J.P. ; van Dam, C.P. Aerodynamic Performance of Thick Blunt Trailing Edge Airfoils. 28th AIAA Applied Aerodynamics Conference, Chicago, Illinois, 2010.
16. Nedić, J. ; Vassilicos, J.C.; Vortex Shedding and Aerodynamic Performance of Airfoil with Multiscale Trailing-Edge Modifications. *AIAA Journal*, **2015**, *53(11)*, 3240-3250.
17. Němec, J. Noise of axial fans and compressors: Study of its radiation and reduction. *Journal of Sound and Vibration*, **1967**, *6(2)*, 230-236.
18. Hubbard, H.H. ; Lansing, D.L. ; Runyan, H.L. A review of rotating blade noise technology. *Journal of Sound and Vibration* , **1971**, *19(3)*, 227-249.
19. Nash, E.C. ; Lowson, M.V. ; McAlpine, A. Boundary-layer instability noise on aerofoils. *J. Fluid Mech.*, **1999**,*382*, 27–61.
20. Simley, E. ; Moriarty, P. ; Palo, S. Aeroacoustic Noise Measurements of a Wind Turbine with BSDS Blades using an Acoustic Array. AIAA Aerospace Sciences Meeting. Orlando. FL., 2010.
21. Manela, A. Nonlinear effects of flow unsteadiness on the acoustic radiation of a heaving airfoil. *Journal of Sound and Vibration*,**2013**, *332(26)*, 7076–7088.
22. Svennberg, U.; Fureby, C. Vortex-Shedding Induced Trailing-Edge Acoustics. 48th AIAA Aerospace Sciences Meeting Including the New Horizons Forum and Aerospace Exposition, Orlando, Florida, 2010.
23. Meher-Homji, C.B. Blading vibration and failures in gas turbines Part B: Compressor and turbine airfoil distress. International Gas Turbine and Aemengine Congress and Exposition, Houston, Texas, 1995.
24. Brooks T.F. ; Hodgson, T.H. Trailing Edge Noise Prediction from Measured Surface Pressure. *Journal of Sound and Vibration*, **1981**,*78*, 69-117.
25. Williams, F.J. ; Hawkings, D. Sound generated by turbulence and surface in arbitrary motion. *Philosophical Transactions of the Royal Society A: Mathematical, Physical & Engineering Sciences*, **1969**, *264(1151)*, 321-342.
26. Blake W.K. and Gershfeld J.L. The Aeroacoustics of Trailing Edges. *Frontiers in Experimental Fluid Mechanics*, **1989**, *46*, 457-532.
27. PRASAD, A. ; WILLIAMSON, C. H. K. The instability of the shear layer separating from a bluff body. *J. Fluid Mech.* ,**1997**, *333*, 375-402.
28. Shannon, D.W. ; Morris, S.C. Experimental investigation of a blunt trailing edge flow field with application to sound generation. *Experiments in fluids*, **2006**, *41(5)*, 777-788
29. Huerre, P. ; Monkewitz P.A.. Local and global instabilities in spatially developing flows. *Annu. Rev. Fluid Mech.* **1990**, *22*, 473– 537
30. Desquesnes, G. ; Terracol, M. ; Sagaut, P. Numerical investigation of the tone noise mechanism over laminar airfoils. *J. Fluid Mech.* **2007**, *591*, 155–182
31. Berg, D.E. ; Zayas, J.R. Aerodynamic and aeroacoustic properties of flatback airfoils. Proceedings of 46th AIAA Aerospace Sciences Meeting and Exhibit. Reno. Nevada. United States, 2008.

32. Kim, T. ; Jeon, M. ; Lee, S. ; Shin, H. Numerical simulation of flatback airfoil aerodynamic noise. *Renewable energy* ,**2014**, *65*, 912-201.
33. Kim, T. ; Lee, S. Aeroacoustic simulations of a blunt trailing-edge wind turbine airfoil. *Journal of Mechanical and Science and Technology*, **2014**, *28(4)*, 1-9.
34. van Dam, C.P. ; Kahn, D.L. Trailing Edge Modifications for Flatback Airfoils. Sandia Report, SAND2008-1781, 2008.
35. Barone, M.F.; Berg, D.E.; Devenport W.J.; Burdisso, R. Aerodynamic and aeroacoustic tests of a flatback version of the DU97-W-300 airfoil. Sandia Report, SAND2009-4185, 2009.
36. Stone, C.; Barone, M.; Smith, M.; Lynch, E. A comparative study of the aerodynamics and aeroacoustics of a flatback airfoil using hybrid RANS-LES. ASME Wind Energy Symposium. Orlando. FL., 2009.
37. Fosas de Pando M.; Schmid, P. J.; Denis Sipp, Tonal noise generation in the flow around an aerofoil: a global stability analysis. 21`eme Congr`es Fran¸cais de M´ecanique, Bordeaux, 2013.
38. Mitchell, B.E.; Lele, S.K.; Moin, P. Direct computation of the sound from a compressible co-rotating vortex pair. *Journal of Fluid Mechanics*, **1995**, *285*, 181–202.
39. Tomoaki, I. ; Takashi, A. ; Shohei, T. Direct simulations of trailing-edge noise generation from two-dimensional airfoils at low Reynolds numbers. *Journal of Sound and Vibration*, **2012**, *331(3)*, 556–574.
40. Schmitt, F.G. About Boussinesq's turbulent viscosity hypothesis: historical remarks and a direct evaluation of its validity. *Comptes Rendus Mécanique*, **2007**, *335(9-10)*, 617-627.
41. Nicoud, F. ; Ducros, F. Subgrid-scale stress modelling based on the square of the velocity gradient tensor. *Flow, Turbulence and Combustion*, **1999**, *62(3)*, 183–200.
42. Lighthill, M.J. On sound generated aerodynamically. 1: general theory. *Proceedings of the Royal Society A: Mathematical, Physical & Engineering Sciences*,**1952**, 211(1107), 564-587.
43. Nitzkorski, Z.; Mahesh, K. A dynamic end cap technique for sound computation using the Ffowcs Williams and Hawkings equations. *Phys. Fluids*,**2014**, *26(115101)*, doi: 10.1063/1.4900876.
44. Brentner, K. S. ; Farassat, F. Analytical Comparison of the Acoustic Analogy and Kirchoff Formulation for Moving Surfaces. *AIAA Journal*, **1998**, *36(8)*, 1379-1386.
45. Brentner, K.S.; Farassat, F. Modeling aerodynamically generated sound of helicopter rotors. *Progress in Aerospace Sciences*, **2003**, *39(2-3)*, 83-120.
46. Star-CCM+ technical manual. 2017.
47. Baggett, J. S. ; Jimenez, J.; Kravchenko, A. G. Resolution requirements in large-eddy simulations of shear flows. Center for Turbulence Research, Annual Research Briefs, NASA Ames. ,**1997**, 51-66.
48. Menter, F.R. Two-equation eddy-viscosity turbulence models for engineering applications. *AIAA journal*, 1994, 32(8), 1598–1605.
49. Kim, S.H.; Bang, H.J.; Shin, H. Design of flatback composite blade for 10MW class wind turbine. 10th International Conference on Composite Science and Technology ICCST/10, 2015.
50. Blake, W.K. Mechanics of flow-induced sound and vibration. Orlando, Florida, USA: Academic Press, Inc; 1986.
51. Brooks, T.F. ; Pope, D.S.; Marcolini, M.A. Airfoil self-noise and prediction. NASA Reference Publication 1218, 1989.